

A rotational ellipsoid model for solid Earth tide with high precision
Yongfeng Yang^{1*}, Yunfei Zhang², Qiang Liu^{2,3}, Xianqing Lv^{2*}, Pu Huang⁴

¹Water Resources Comprehensive Development Center, Bureau of Water Resources of Shandong Province, Jinan, 250013, China

²Frontier Science Center for Deep Ocean Multispheres and Earth System (FDOMES), Physical Oceanography Laboratory, Ocean University of China, Qingdao 266100, China

³College of Engineering, Ocean University of China, Qingdao 266100, China

⁴National Laboratory of Solid State Microstructures and Department of Physics, Nanjing University, Nanjing 210093, China

*Corresponding author: Yongfeng Yang (roufeng_yang@outlook.com);

Xianqing Lv (xqinglv@ouc.edu.cn)

Abstract

Solid Earth tide represents the elastic response of solid Earth to the lunar (solar) gravitational force. The yielding solid Earth due to the force has been thought to be a prolate ellipsoid since the time of Lord Kelvin, yet the ellipsoid's geometry such as semi-major axis's length, semi-minor axis's length, and oblateness remains unresolved. Additionally, the tidal displacement of solid Earth is conventionally resolved through a combination of expanded potential equations and given Earth model. Here we present a geometric model in which both the ellipsoid's geometry and the tidal displacement of solid Earth can be resolved through a rotating ellipse with respect to the Moon (Sun). We test the geometric model using 23-year gravity data from 22 superconducting gravimeter (SG) stations and compare it with the current model recommended by the IERS (International Earth Rotation System) conventions (2010), the average Root Mean Square (*RMS*) deviation of the gravity change yielded by the geometric model against observation is 6.47 μGal (equivalent to 2.07 cm), while that yielded by the current model is 30.77 μGal (equivalent to 9.85 cm). The geometric model represents a significant advance in understanding and predicting solid Earth tide, and will greatly contribute to many application fields such as geodesy, geophysics, astronomy, and oceanography.

Keywords Solid Earth tide, geometry of ellipsoid, tidal displacement, SG gravity

1 Introduction

Tides are typical manifestations of the Earth's systems in response to the gravitational force of the Moon and Sun (Melchior 1983; Pugh 2014). The elastic response of solid Earth to the force is called body tide or solid Earth tide. Not like ocean tide that is rather spectacular, solid Earth tide is more difficult to observe due to the movement of the reference frame of the observer (Lau and Schindelegger 2023; Sutterley et al. 2017). Even so, the tidal signal of solid Earth can be captured with instruments such as horizontal pendulum, tide gauge, gravimeter, Very Long Baseline Interferometry (VLBI), Global Positioning System (GPS) (Khan and Tscherning 2001; Krásná et al. 2012; Milne 1910; Petrov and Ma 2003; Sutterley et al. 2017; Yuan et al. 2013), diamagnetic-levitated micro-oscillator (Leng et al. 2024), and so on.

A theoretical treatment of solid Earth tide commonly incorporates the expanded potential equations and given Earth model to resolve the dimensionless Love-Shida numbers (Lau and Schindelegger 2023; Love 1911; Melchior 1983; Shida 1912). The Love-Shida numbers represent the ratios between the observation under the forcing and the expectation in the equilibrium tide theory. The existing solid Earth tide theory has been developed into model (Defraigne et al. 1996; Dehant et al. 1999; Mathews et al. 1995) and highly recommended by the IERS (Gérard and Luzum 2010). The tidal displacement computed by the current model is being widely utilized for the correction on the deflection of the vertical (DOV), satellite orbit, the Interferometric Synthetic Aperture Radar image, tectonic velocity, glacial isostatic adjustment, Global Seismographic Network, and vertical land motion at tide gauge (Bos et al. 2015; Davis and Berger 2007; Herrmann and Bucksch 2014; Montenbruck et al. 2002; Woodworth et al. 2017; Xu 2010; Xu and Sandwell 2020). The tidal displacement computed by the model is also subtracted from the measured sea surface height when ocean tide models are created (Fok 2013). Solid Earth tide may help reveal the Earth's interior structure (Ito & Simons, 2011), the Earth's response to ocean tide loading (Bos et al. 2015), and the correlation between Earthquake and tidal stress (Agnew 2007). Solid Earth tide computed has been the key for understanding sea level change and variability (Filmer et al. 2020; Wöppelmann and Marcos 2016), and has been fundamental for establishing

the International Celestial Reference Frame (ICRF) (Altamimi et al. 2002), the International Terrestrial Reference Frame (ITRF) (Ma et al. 1998), and Geopotential (Mathews et al. 2002). Since the time of Lord Kelvin, it has been believed that the yielding solid Earth due to the lunar (solar) gravitational force is a prolate ellipsoid, in which solid Earth is slightly elongated along the Earth-Moon (Sun) line and shortened around the parts remote from the elongation (Love 1909). Nevertheless, the ellipsoid's geometry such as semi-major axis's length, semi-minor axis's length, and oblateness are unresolved. The existing solid Earth tide theory has been tested. Most of these studies (Baker and Bos 2003; Melchior 1994; Scherneck 1991) making comparison of theory and observation are limited to the gravimetric factor of specific tidal constituents (e.g., O_1 , M_2 , P_1 , and K_1). A tidal constituent is a mathematical expression for the tidal force, and O_1 , P_1 and K_1 are the dominant diurnal constituents, while M_2 is one of the semidiurnal constituents. The gravimetric factor is a ratio of the observation and expectation and itself is a linear combination of the Love-Shida numbers (Krásná et al. 2012). Different from this routine, Goodkind (Goodkind 1996) constructed two theoretical tide time series plus the local barometric pressure time series to fit the gravimeter signal in order to determine three scalar parameters. Practically, the tidal displacement of a site is treated as a sum of the displacements of all tidal constituents, and the displacement of each constituent is computed through a cosine function that is incorporated by the amplitude factor, the amplitude, and the phase lag. The number of the tidal constituents selected for tidal displacement prediction often reaches tens or hundreds or more. From this side, a comparison of the gravimetric factor doesn't relate to the tidal displacement, and consequently, the accuracy of tidal displacement predicted by the existing theory remains unclear.

Superconducting gravimeter (SG) data provide the most accurate information about solid Earth tide (Voigt et al. 2016; Xu 2010). A detailed description of SGs and their measurements may refer to this book (Xu 2010). More than 40 SG stations are presently included in the network of International Geodynamics and Earth Tide Service (IGETS), and their time series cover more than 25 years. The IGETS gravity data are globally available through open access (Boy et al. 2023; Voigt et al. 2016), and some of them have been used for creating local tide models using harmonic analysis (Hinderer et al. 2020; Xu et al. 2020; Xu et al. 2004), and their adaptability was well discussed (Sun et al. 2005).

2 Geometric Solid Earth Tide Model

The Earth can be considered as a solid sphere with a thicker core, encompassed by a thinner layer of water and atmosphere (Fowler 1990). This approximation allows to neglect any material variations within the Earth and any discrepancies in radius, assuming it to be a symmetrical, rotating, elastic, homogeneous, and oceanless sphere. The Earth participates in two curved motions in the solar system: one is the Earth orbiting around the barycenter of the Earth-Moon system and the other is the Earth-Moon system orbiting around the Sun (Fig. 1(a)). A fuller description of the motions of the Earth, Moon, and Sun can be found in these works (Kopal 1969; Roy 1978). Mechanically, the two curved motions generate two centrifugal forces, f_1 and f_2 , for solid Earth. Please note, the centrifugal force is inertia other than the real force. These two centrifugal forces f_1 and f_2 are counterbalanced by the gravitational force F_1 from the Moon and gravitational force F_2 from the Sun, respectively. It is these force balances that enable the Earth to steadily move around the barycenter of the Earth-Moon system and around the Sun. The Earth's response to a combination of these opposing forces f_1 (f_2) and F_1 (F_2) slightly elongates the Earth's body along the Earth-Moon (Sun) line and shortens the body midway (Fig. 1(b and c)). We assume that the deformation can be represented with a prolate ellipsoid whose major axis points to the Earth-Moon (Sun) line and center coincides with the center of the Earth.

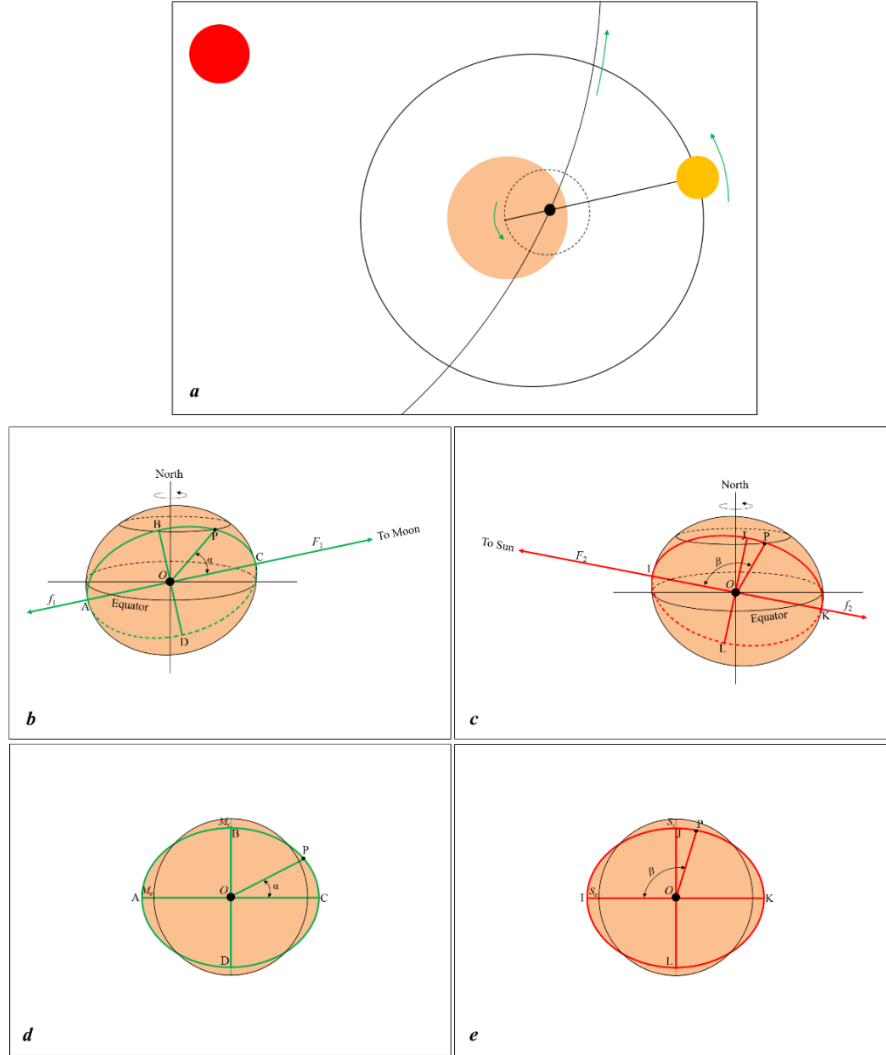


Figure 1. Combined effect of opposing forces on solid Earth. (a) the Earth's motions around the barycenter of the Earth-Moon system and around the Sun. (b and c) the resultant prolate ellipsoid due to a combination of the two opposing forces, i.e., centrifugal forces f_1 (f_2) and gravitational force F_1 (F_2). α and β are the lunar and solar angles of site P relative to the Earth's center O , respectively. (d and e) the sections dissected from the prolate ellipsoid passing site P and the major axis AC (IK). Black circle denotes the original shape of section ABCD (IJKL). M_e (S_e) and M_s (S_s) denote the elongation and shortening in the prolate ellipsoid due to the Moon (Sun), respectively.

As exhibited in Figure 1(b(c)), at the moment we use a section that passes a site and the prolate ellipsoid's major axis to cut the ellipsoid's body, the resultant intersection line at the ellipsoid's surface would be an ellipse. As the Earth spins around its axis, the site is entrained to move. The

relative positions between the site, the Earth's center, and the Moon are timely varying. After a period of time, we use a section that passes the site and the prolate ellipsoid's major axis to cut the ellipsoid's body again, the resultant intersection line at the ellipsoid's surface would be another ellipse. We find, at any time the resultant intersection line at the ellipsoid's surface due to the cutting would be an ellipse. Consequently, the distance of the site from the Earth's center can be expressed through a geometry of the ellipse (Fig. 1(*d* and *e*)). Taking into account the co-existence of the two prolate ellipsoids due to the Moon and Sun, the combined vertical displacement of site P relative to the Earth's center can be written as $H=H_m+H_s$, where

$$\begin{aligned} H_m &= \sqrt{(R + M_e)^2 \cos^2 \alpha + (R - M_s)^2 \sin^2 \alpha} - R \\ H_s &= \sqrt{(R + S_e)^2 \cos^2 \beta + (R - S_s)^2 \sin^2 \beta} - R \end{aligned} \quad (1)$$

Where H_m (H_s) is the vertical displacement of a site relative to the Earth's center in the prolate ellipsoid due to the Moon (Sun). R is the mean radius of solid Earth, M_e (S_e) and M_s (S_s) are the elongation and shortening in the prolate ellipsoid due to the Moon (Sun), respectively. $(R+M_e)$ and $(R-M_s)$ are the semi-major axis's length and semi-minor axis's length of the ellipsoid due to the Moon, whereas $(R+S_e)$ and $(R-S_s)$ are the semi-major axis's length and semi-minor axis's length of the ellipsoid due the Sun. α and β are the lunar and solar angles of site P relative to the Earth's center, and they can be calculated through a standard formula in spherical trigonometry (Smart 1940): $\cos \alpha = \sin \sigma \sin \delta_m + \cos \sigma \cos \delta_m \cos C_{mm}$, $\cos \beta = \sin \sigma \sin \delta_s + \cos \sigma \cos \delta_m \cos C_{ms}$. Where σ , δ_m , δ_s , C_{mm} , and C_{ms} are the geographic latitude of site P, the declination of the Moon, the declination of the Sun, the hour angle of site P with respect to the Moon, and the hour angle of site P with respect to the Sun, respectively.

M_e (S_e) and M_s (S_s) can be developed into $M_e = K_{me} P_m \cos^2 \delta_m$ ($S_e = K_{se} P_s \cos^2 \delta_s$) and $M_s = K_{ms} P_m \cos^2 \delta_m$ ($S_s = K_{ss} P_s \cos^2 \delta_s$), where $P_m = D_{me}^2 / D_m^2$ ($P_s = D_{se}^2 / D_s^2$) is a distance factor that relates to the Earth and Moon (Sun), D_{me} (D_{se}) is the mean distance between the Earth and Moon (Sun), D_m (D_s) is the temporary distance between the Earth and Moon (Sun). K_{me} (K_{se}) and K_{ms} (K_{ss}) are undetermined parameters of elongation and shortening in the prolate ellipsoid due to the Moon (Sun), $\cos^2 \delta_m$ ($\cos^2 \delta_s$) denotes a latitude factor that relates to the position of the Moon (Sun).

Equation (1) indicates that, if the vertical displacement of a site is measured, we may use the measured data as input and take a least-squares fitting to resolve the undetermined parameters K_{me} (K_{se}) and K_{ms} (K_{ss}). Furthermore, the elongation M_e (S_e) and the shortening M_s (S_s) in the prolate ellipsoids can be determined with these known parameters and ephemeris data.

The vertical displacement of a site can be measured by GPS whose positioning precision has presently reached a millimeter level with a static solution (Xu 2010). But if a dynamic solution is applied, the precision will be only in one centimetre level (Xu 2007), which is not good for resolving these parameters. Instead, the vertical displacement corresponds to gravity change, and gravity change has been widely measured by SGs whose precision is less than $0.05\mu\text{Gal}$, and therefore, the gravity change data are ideal for resolving these parameters. The measured gravity change as a whole include the effects caused by solid Earth tide, atmosphere pressure, pole motion, ocean tide loading, and so on (Xu 2010). This means that the gravity change caused by solid Earth tide is only suitable for the solution of our model. Here, we select time series of four SG stations (Canberra, Bad Homburg, Apache Point, and Sutherland) from IGETS (Voigt et al. 2016), and these stations are located in Australia, Europe, America, and Africa, respectively. The gravity data in IGETs are recorded with three levels: the level 1 are raw without any correction, the level 2 are corrected for instrumental perturbations, and the level 3 are those after particular geophysical corrects had been separated into solid Earth tide, atmosphere load, rotation, drift, ocean tide loading, residuals, and so on (Voigt et al. 2016). This separation allows us to directly utilize the gravity change caused by solid Earth tide. The time covering of the selected time series is from August 1, 2014, to December 30, 2014. The latitude and longitude of these stations are listed in Table 1. As the unit of gravity change differs from that of vertical displacement, a transformation between two kinds of data was considered. The transformation from vertical displacement to gravity change can be approximately expressed as

$$\Delta g = (1/(H + R)^2 - 1/R^2)GM_e \quad (2)$$

where H and Δg are vertical displacement and its resultant gravity change, respectively. G , M_e , R are the gravitational constant, mass of the Earth, and the mean distance of a SG station from the Earth's center, respectively. We here assume that the mean distance is equal to the Earth's mean radius. $G = 6.67 \times 10^{-11} \text{m}^1 \text{s}^{-2}$, $M_e = 5.97 \times 10^{24} \text{kg}$ (Luzum et al. 2011), and $R = 6371 \text{km}$ (Lide 2000). In the equation (2), we use the Earth's mean radius to replace the mean distance of a SG station from the Earth's center, but the mean distance is not equal to the Earth's mean radius, this replacement deserves a discussion. When $R = 6356 \text{km}$ (if the SG station's mean distance is equal to the pole radius) or $R = 6378 \text{km}$ (if the SG station's mean distance is equal to the equator radius), for a vertical displacement $H=0.6 \text{m}$, the equation (2) can result in a gravity change error of $-1.31 \mu\text{Gal}$ or $0.61 \mu\text{Gal}$ relative to the vertical displacement computed with the Earth's mean distance

$R = 6371$ km. Most of the SG stations in the network of IGETS have gravity change of greater than $100 \mu\text{Gal}$, the gravity change error computed through the equation above is on one microgal level and therefore can be neglected.

Ephemeris data, including the declination of the Moon (Sun) and the average and temporary distance of the Moon (Sun) from Earth, were obtained from NASA JPL horizons system. The fitted results for K_{me} , K_{ms} , K_{se} , and K_{ss} are 41.33 cm, 21.41 cm, 15.93 cm, and 13.03 cm, respectively. Taking into account the varying inclination of the Moon (Sun) and the temporary distance between the Earth and Moon (Sun), we estimate that during a period of time (from 1990 to 2030), the elongation M_e (S_e) and shortening M_s (S_s) of solid Earth due to the Moon (Sun) range from 49.75 cm to 29.77 cm (16.09 cm to 12.98 cm) and from 25.77 cm to 15.42 cm (13.16 cm to 10.62 cm), respectively. The variations of M_e , M_s , S_e , and S_s are typically compared in Fig. 2. Given the Earth's mean radius $R=6371000.00$ m, the semi-major axis's length and semi-minor axis's length in the ellipsoid due to the Moon vary from 6371000.50 m to 6371000.30 m and from 6370999.85 m to 6370999.74 m, and the semi-major axis's length and semi-minor axis's length in the ellipsoid due to the Sun vary from 6371000.16 m to 6371000.13 m and from 6370999.89 m to 6370999.87 m. The oblateness of an ellipsoid is written as $f=(a-c)/c$, where f , a , and c are the oblateness of the ellipsoid, the semi-major axis's length, and the semi-minor axis's length, respectively. As a result, the oblateness for the ellipsoid due to the Moon (Sun) ranges from $7.09 \cdot 10^{-8}$ ($3.71 \cdot 10^{-8}$) to $11.85 \cdot 10^{-8}$ ($4.59 \cdot 10^{-8}$).

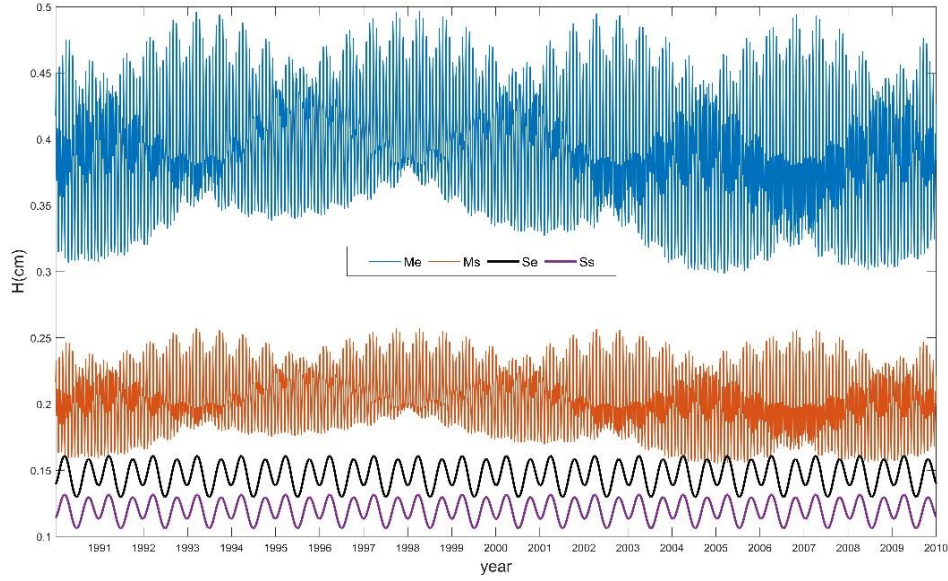


Figure 2. Variations of the elongation M_e (S_e) and shortening M_s (S_s) of solid Earth from 1990 to 2010. M_e (S_e) and M_s (S_s) are calculated through $M_e=K_{me}P_m\cos^2\delta_m$ ($S_e=K_{se}P_s\cos^2\delta_s$) and $M_s=K_{ms}P_m\cos^2\delta_m$ ($S_s=K_{ss}P_s\cos^2\delta_s$), and P_m and P_s are the distance factors that relates to the Earth and Moon (Sun), D_{me} (D_{se}) are the mean distance between the Earth and Moon (Sun), D_m (D_s) is the temporary distance between the Earth and Moon (Sun).

Taking the equation (1) and ephemeris data, one may compute the tidal displacement of any site on the Earth's surface at any time. Gravity data of 22 SG stations from IGETS are used to test the geometric model. Similarly, the gravity change caused by solid Earth tide are selected from the level 3 of the IGETs. These stations are located around the world, ensuring their representativeness within the network. The selected time series of each of these stations have a continuous coverage of 6 months, and the total covering of the selected data spans from January 1998 to June 2021. To examine the strength of the geometric model, we compare it with the current solid Earth tide model recommended by the IERS conventions (2010). The current model has been developed/incorporated into some softwares such as Solid (Milbert 2018), pyTMD (Sutterley et al. 2017), and Etideload (Zhang et al. 2021). Solid is an implementation of the solid earth tide computation documented in the IERS Conventions (2003). The solid Earth tide computation incorporated in pyTMD is based on the IERS conventions (2010). Since the solid Earth tide computation documented in the IERS conventions (2003) is identical to that documented in the IERS conventions (2010), the solid Earth tide computed by Solid is equivalent to that computed

by pyTMD. The solid Earth tide computation incorporated in Etideload is mostly based on the IERS conventions (2010), but the effect of planets on Earth tide is included. Hence, we select Solid and pyTMD as representative of the current model. The solid Earth tide computed by the current model is displacement, too. For a convenience in comparison, we use the equation (2) to transform the vertical displacement computed by the geometric model and the current model into gravity change.

The *RMS* deviation for a SG station can be written as follows

$$RMS = \sqrt{\sum_i^m (g_m(i) - g_o(i))^2 / m} \quad (3)$$

where $g_m(i)$ represents the gravity change computed by the geometric model or the current model (Solid (pyTMD) and Etideload), $g_o(i)$ represents the observed gravity change at the SG station, and m is the total number of observations used in the analysis. The detailed information of the selected time series of these stations and the *RMS* deviation of various models are listed in Table 1.

Table 1. Time series of 22 SG stations and the *RMS* deviation of various models against observation

SG Station	Latitude	Longitude	Time Span	<i>RMS</i> (μ Gal)		
				Etideload	Solid (pyTMD)	Geometric Model
Vienna	48.25°	16.36°	19980101-19980630	27.82	27.97	4.92
Wuhan	30.52°	114.49°	19980101-19980630	31	31.48	5.53
Apache Point	32.78°	254.18°	20160101-20160630	29.98	30.55	5.3
Conrad	47.93°	15.86°	20160101-20160630	27.09	27.68	4.84
Lhasa	29.65°	91.04°	20160101-20160630	30.79	31.26	5.2
Lijiang	26.90°	100.23°	20160101-20160630	31.96	32.35	5.5
La Plata	-34.87°	301.86°	20180101-20180630	27.21	27.77	5.02
Medicina	44.52°	11.65°	20180101-20180630	30.94	31.56	6.4
Rochefort	50.16°	5.23°	20180101-20180630	28.6	29.19	5.65
Schiltach	48.33°	8.33°	20180101-20180630	28.51	29.05	5.52
Aubure	48.22°	7.20°	20210101-20210630	28.46	29.03	5.54
Bad Homburg	50.23°	8.61°	20210101-20210630	30.48	31.49	7.34
Canberra	-35.32°	149.01°	20210101-20210630	31.69	32.55	8.65

Cantley	45.59°	284.19°	20210101-20210630	30.95	32.07	8.08
Helgoland	54.18°	7.89°	20210101-20210630	29.98	30.83	6.18
Larzac	43.97°	3.22°	20210101-20210630	30.33	31.38	7.63
Onsala	57.39°	11.93°	20210101-20210630	31.61	32.32	6.25
Pecny	49.91°	14.79°	20210101-20210630	30.57	31.54	7.14
Rustrel	43.94°	5.48°	20210101-20210630	30.44	31.49	7.66
Strasbourg	48.62°	7.68°	20210101-20210630	30.45	31.45	7.26
Sutherland	-32.38°	20.81°	20210101-20210630	32.03	32.88	9.09
Yebes	40.52°	356.91°	20210101-20210630	30.05	31.11	7.72
Mean				30.04	30.77	6.47

We find that the geometric model is significantly superior to the existing models, the average *RMS* deviation of the gravity change computed by the geometric model against observation across the 22 SG stations is 6.47 μGal , the average *RMS* of the gravity change computed by Solid (pyTMD) is 30.77 μGal , while the average *RMS* of the gravity change computed by Etideload is 30.04 μGal . One microgal of gravity change is equivalent to about 3.2 mm of relative height change (Ito et al., 2009), these *RMS* deviations of gravity change thereby correspond to height change of 2.07 cm, 9.85 cm, and 9.61 cm, respectively. The comparison is typically displayed with four SG stations (Vienna, Aubure, Apache Point, and La Plata) (Fig. 3), showing that the gravity change computed by the geometric model is more consistent with observed data than the existing models. The gravity change computed by the current model is overwhelmingly less than the observed gravity change, and at the time of high tide, the difference between the two may rise up to 70 μGal (equivalent to about 22 cm).

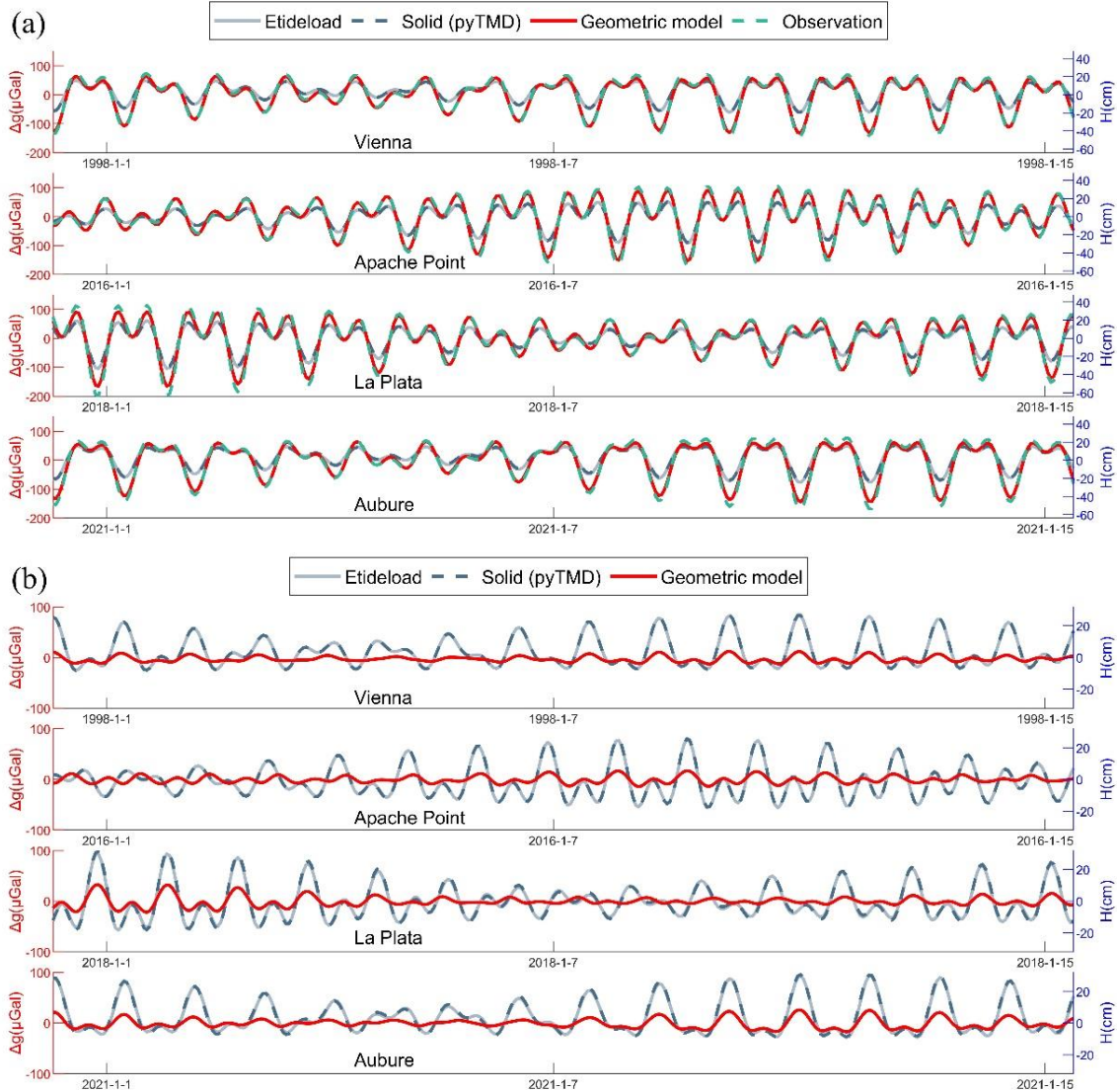


Figure 3. Gravity change comparison between various models. (a) Gravity change computed by the models at four SG stations. (b) Gravity change difference between the models and observation.

We show that from 1990 to 2030, the averaged M_e is about 2.7 times of the average S_e , and the averaged M_s is about 1.7 times of the average S_s . These ratios determine solid Earth to be dominantly elongated along the Earth-Moon line and shortened around the parts remote from the elongation. This geometry of deformation requires, if a site enters the elongation, it will experience a fall in gravity, and if the site enters the shortening, it will experience an increase in gravity. To examine this expectation, we construct a correlation between lunar angle and gravity variation for 20 SG stations (Fig. 4). Results uniformly indicate a decline in gravity during lunar angles of 0° -

45° and 135°- 180°, while an increase in gravity during lunar phases of 45°-135°, supporting the existence of the elongated solid Earth.

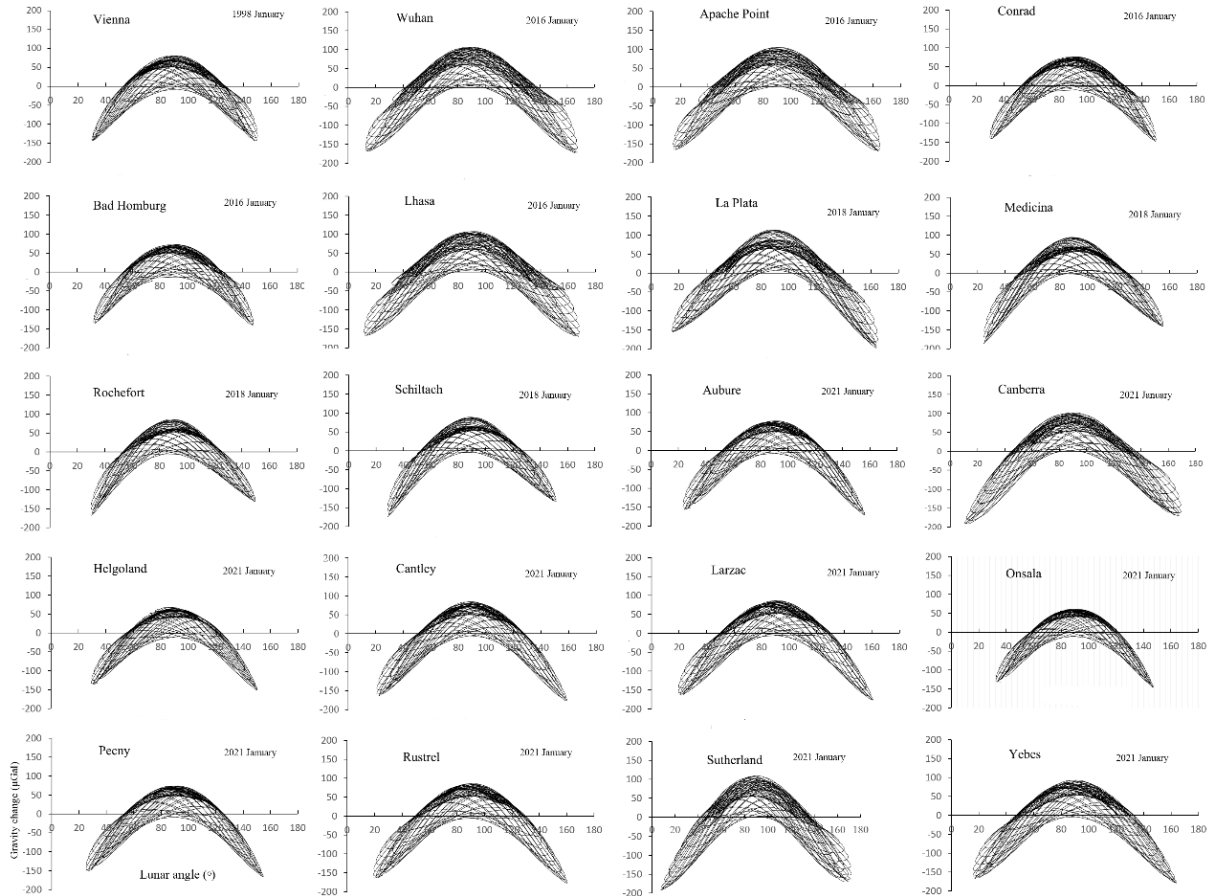


Figure 4. Gravity change out to lunar angle. Gravity data of 20 SG stations are selected from IGETs (Voigt et al. 2016). Lunar angle is the angle of the SG station and the Moon relative to the Earth’s center.

3 Discussion

Essentially, the current model uses the tidal force (potential) and the response of solid Earth to it (i.e., the Love-Shida numbers) to resolve the tidal displacement. Due to the spatial variation of the tidal force, and due to the complexity of the Earth’s structure and the materials within it, a precise understanding of the response is hard to reach. Moreover, the Love-Shida numbers are only constrained by limited observations, this cannot guarantee their adaptability for a global scale. Hence, the current model would be difficult to realize a high accuracy of tidal displacement prediction. This issue may find reference from astronomy. The Copernicus’s heliocentric model

presented that the planets are revolving around the Sun, not the other way around. However, the details of these movements, such as their distance from the Sun and orbital speed, remained unclear until the birth of Kepler's model of elliptical orbit. Although the elliptical orbit is a manifestation of the gravitation force, it is difficult to use the force and the response of planet to it to resolve the movement of planet because the response is rather complicated.

The low accuracy of the current model has imposed challenge on its application. It is reported that the best ocean tide models available today have the accuracy of a few centimeters in open ocean (Stammer et al. 2014). In creating these models, the solid Earth tide computed by the current model is firstly subtracted from the measured sea surface height so as to obtain the observed ocean tide. The observed ocean tide is obtained through an expression as $\Delta h = h_{ss} - h_v - h_m$, where h_{ss} , h_v , and h_m represent the measured sea surface height, solid Earth tide computed by the current model, and mean sea surface, respectively (Fok 2013). Hence, the observed ocean tide obtained through the expression is overestimated by 9.0 cm due to the inadequacy of the current model. Further, the observed ocean tide is used to resolve the parameters of tidal constituents, with these known parameters, the ocean tide model is eventually built and used to make prediction. Our demonstration of ocean tide model reveals that the accuracy of a few centimeters for the best ocean tide models cannot be realistic. NOAA Climate.gov recently reported that the rate of global sea level rise has increased from 1.4 mm per year throughout most of the twentieth century to 3.6 mm per year from 2006–2015. The sea level rise is determined through tide gauge and satellites that relate to vertical land motion, and the vertical land motion is corrected by the solid Earth tide computed by the current model. For accurate determination of sea level change, vertical land motion is required to have standard errors that are 1 order of magnitude lower than the contemporary climate signals of 1 to 3 mm/yr observed on average in sea level records from tide gauges or satellites (Wöppelmann and Marcos 2016). Inadequate correction of solid Earth tide on vertical land motion may flood a vertical land motion of a few millimeters per year. It is no doubt, the low accuracy of the current model may discount any of precise ground- and spatial-based measurements. These results suggest that the various fields which have utilized the current model need to be reevaluated.

4 Conclusions

The yielding Earth due to the lunar (solar) gravitational force is long thought to be a prolate ellipsoid, in which solid Earth is slightly elongated along the Earth-Moon (Sun) line and shortened around the parts remote from the elongation. Yet, the ellipsoid's geometry such as semi-major axis's length, semi-minor axis's length, and oblateness remains unresolved. Additionally, the tidal displacement of solid Earth is conventionally resolved through a combination of expanded potential equations and given Earth model. In this study, we represent a geometric model in which both the geometry of ellipsoid and the tidal displacement of solid Earth can be resolved through a rotating ellipse with respect to the Moon (Sun). We find that during a period of time (from 1990 to 2030), the ellipsoid's oblateness due to the lunar (solar) gravitational force varies from 7.09×10^{-8} (3.71×10^{-8}) to 11.85×10^{-8} (4.59×10^{-8}). We test the geometric model using 23-year gravity data from 22 superconducting gravimeter (SG) stations and compare it with the current model recommended by the IERS (International Earth Rotation System) conventions (2010), the average Root Mean Square (*RMS*) deviation of the gravity change yielded by the geometric model against observation is $6.47 \mu\text{Gal}$ (equivalent to 2.07 cm), while that yielded by the current model is $30.77 \mu\text{Gal}$ (equivalent to 9.85 cm). The geometric model represents a significant advance in understanding and predicting solid Earth tide, and will greatly contribute to many application fields such as geodesy, geophysics, astronomy, and oceanography.

Acknowledgments: Authors declare that they have no competing interests. This research was supported by the National Natural Science Foundation of China (Grant No. 42076011) and the National Key Research and Development Program of China (Grant No.2022YFC3105003). We thank Tyler C. Sutterley, Mao Zhou, and Chuanyin Zhang for help in producing solid earth tide data through different softwares, and Jean-Paul Boy for help in obtaining superconducting gravimeter data from IGETS. The authors are very grateful to Jon Giorgini for help in extracting ephemeris data from NASA JPL horizons system. The authors are also grateful to Dennis Milbert for his clarification of the IERS conventions and Solid earth tide software, and to Heping Sun, Gerhard Jentzsch, and Christian Voigt for their valuable comments.

Author Contributions: YFY conceived the model and drafted the manuscript. YFZ and YFY contributed to the parameter fitting and validation of the model. QL and PH carried out the logical

and expressive modifications of the paper and actively engaged in discussions throughout the progress of the paper. XQL was responsible for the overall planning of the research and improved the model. All authors participated in the revision of the paper.

Data Availability Statement: The superconducting gravity data used in this research are available through Voigt et al., 2016 (<ftp://igetsftp.gfz-potsdam.de>). The ephemeris data used are obtained from NASA JPL horizons system.

References

- Agnew DC (2007) Earth Tides. *Treatise on Geophysics: Volume 1-10* 1–10:163–195. <https://doi.org/10.1016/B978-044452748-6.00056-0>
- Altamimi Z, Sillard P, Boucher C (2002) ITRF2000: A new release of the International Terrestrial Reference Frame for earth science applications. *J Geophys Res Solid Earth* 107:. <https://doi.org/10.1029/2001jb000561>
- Baker TF, Bos MS (2003) Validating earth and ocean tide models using tidal gravity measurements. *Geophys J Int* 152:. <https://doi.org/10.1046/j.1365-246X.2003.01863.x>
- Bos MS, Penna NT, Baker TF, Clarke PJ (2015) Ocean tide loading displacements in western Europe: 2. GPS-observed anelastic dispersion in the asthenosphere. *J Geophys Res Solid Earth* 120:. <https://doi.org/10.1002/2015JB011884>
- Boy JP, Barriot JP, Förste C, et al (2023) Achievements of the First 4 Years of the International Geodynamics and Earth Tide Service (IGETS) 2015–2019. In: *International Association of Geodesy Symposia*
- David R. Lide J (2000) *CRC handbook of chemistry and physics, 2000-2001*
- Davis P, Berger J (2007) Calibration of the Global Seismographic Network Using Tides. *Seismological Research Letters* 78:454–459. <https://doi.org/10.1785/GSSRL.78.4.454>
- Defraigne P, Dehant V, Wahr JM (1996) Internal Loading of an Inhomogeneous Compressible Earth With Phase Boundaries. *Geophys J Int* 125:173–192. <https://doi.org/10.1111/J.1365-246X.1996.TB06544.X>
- Dehant V, Defraigne P, Wahr JM (1999) Tides for a convective Earth. *J Geophys Res Solid Earth* 104:1035–1058. <https://doi.org/10.1029/1998JB900051>

- Filmer MS, Williams SDP, Hughes CW, et al (2020) An experiment to test satellite radar interferometry-observed geodetic ties to remotely monitor vertical land motion at tide gauges. *Glob Planet Change* 185:. <https://doi.org/10.1016/j.gloplacha.2019.103084>
- Fowler CMR (1990) *The solid earth: an introduction to global geophysics*. Cambridge University Press. <https://doi.org/10.1029/90eo00309>
- Fok, M.S, Hok Sum. BS (2013) *Ocean Tides Modeling using Satellite Altimetry*. *J Chem Inf Model* 53:
- Gérard P, Luzum B (2010) *IERS Conventions (2010)*. Bureau International Des Poids Et Mesures Sevres (France)
- Goodkind JM (1996) Test of theoretical solid earth and ocean gravity tides. *Geophys J Int* 125:. <https://doi.org/10.1111/j.1365-246X.1996.tb06537.x>
- Guo J, Jin X, Bian S, Chang X (2022) Corrections of solid earth tide and ocean tide for measurement of deflection of the vertical. *Cehui Xuebao/Acta Geodaetica et Cartographica Sinica* 51:. <https://doi.org/10.11947/j.AGCS.2022.20220104>
- Herrmann H, Bucksch H (2014) *Dictionary Geotechnical Engineering/Wörterbuch GeoTechnik*
- Hinderer J, Riccardi U, Rosat S, et al (2020) A study of the solid earth tides, ocean and atmospheric loadings using an 8-year record (2010–2018) from superconducting gravimeter OSG-060 at Djougou (Benin, West Africa). *J Geodyn* 134:. <https://doi.org/10.1016/j.jog.2019.101692>
- Ito T, Okubo M, Sagiya T (2009) High resolution mapping of Earth tide response based on GPS data in Japan. *J Geodyn* 48:. <https://doi.org/10.1016/j.jog.2009.09.012>
- Ito T, Simons M (2011) Probing asthenospheric density, temperature, and elastic moduli below the western United States. *Science* (1979) 332:. <https://doi.org/10.1126/science.1202584>
- Khan SA, Tscherning CC (2001) Determination of semi-diurnal ocean tide loading constituents using GPS in Alaska. *Geophys Res Lett* 28:2249–2252. <https://doi.org/10.1029/2000GL011890>
- Kopal Z (1969) Dynamics of the Earth-Moon System. *The Moon* 55–68. https://doi.org/10.1007/978-94-010-3408-1_6
- Krásná H, Böhm J, Böhm S., and Schuh H (2012) Solid Earth Tide Parameters from VLBI Measurements and FCN Analysis. In: *IVS 2012 General Meeting Proceedings*, 405–409. https://www.researchgate.net/publication/265794235_Solid_Earth_Tide_Parameters_from_VLBI_Measurements_and_FCN_Analysis. Accessed 18 Jan 2024

- Lau HCP, Schindelegger M (2023) Solid Earth tides. *A Journey Through Tides* 365–387. <https://doi.org/10.1016/B978-0-323-90851-1.00016-9>
- Leng Y, Chen Y, Li R, et al (2024) Measurement of the Earth Tides with a Diamagnetic-Levitated Micro-Oscillator at Room Temperature. *Phys Rev Lett* 132:. <https://doi.org/10.1103/PhysRevLett.132.123601>
- Love AEH (1911) *Some Problems of Geodynamics*. In: The University Press. 10.1016/B978-044452748-6.00056-0.
- Love AEH (1909) The yielding of the Earth to disturbing forces. *Mon Not R Astron Soc* 69:. <https://doi.org/10.1093/mnras/69.6.476>
- Luzum B, Capitaine N, Fienga A, et al (2011) The IAU 2009 system of astronomical constants: The report of the IAU working group on numerical standards for Fundamental Astronomy. *Celest Mech Dyn Astron* 110:. <https://doi.org/10.1007/s10569-011-9352-4>
- Ma C, Arias EF, Eubanks TM, et al (1998) The International Celestial Reference Frame as Realized by Very Long Baseline Interferometry. *Astron J* 116:. <https://doi.org/10.1086/300408>
- Mathews PM, Buffett BA, Shapiro II (1995) Love numbers for a rotating spheroidal Earth : : New definitions and numerical values. *Geophys Res Lett* 22: 579–582. <https://doi.org/10.1029/95GL00161>
- Mathews PM, Herring TA, Buffett BA (2002) Modeling of nutation and precession: New nutation series for nonrigid Earth and insights into the Earth’s interior. *J Geophys Res Solid Earth* 107:. <https://doi.org/10.1029/2001jb000390>
- Melchior, P. (1983) *The tides of the planet earth*. Pergamon Press, Oxford
- Milbert D (2018) Solid, <https://geodesyworld.github.io/SOFTS/solid.htm>
- Milne J (1910) Surface Deformation and the Tides. *Nature* 82: 427. <https://doi.org/10.1038/082427a0>
- Montenbruck O, Gill E, Lutze F (2002) *Satellite Orbits: Models, Methods, and Applications*. *Appl Mech Rev* 55:B27–B28. <https://doi.org/10.1115/1.1451162>
- Petrov L, Ma C (2003) Study of harmonic site position variations determined by very long baseline interferometry. *J Geophys Res Solid Earth* 108:2190. <https://doi.org/10.1029/2002JB001801>
- Pugh DT, and WPL (2014) *Sea-Level Science: Understanding Tides, Surges, Tsunamis and Mean Sea-Level Changes*. In: Cambridge Univ. Press. Cambridge.

- Roy AE (1978) *Orbital Motion*. In: Adam Hilger, Bristol. Accessed 18 Jan 2024
- Scherneck H -G (1991) A parametrized solid earth tide model and ocean tide loading effects for global geodetic baseline measurements. *Geophys J Int* 106:. <https://doi.org/10.1111/j.1365-246X.1991.tb06339.x>
- Smart WM (1940) *Spherical Astronomy* -. In: Cambridge University Press. Accessed 18 Jan 2024
- Stammer D, Ray RD, Andersen OB, et al (2014) Accuracy assessment of global barotropic ocean tide models. *Reviews of Geophysics* 52
- Sun H, Ducarme B, Xu H, et al (2005) Adaptability of the ocean and earth tidal models based on global observations of the superconducting gravimeters. *Sci China Ser D Earth Sci* 48:. <https://doi.org/10.1360/04yd0071>
- Sutterley, T. C., Alley, K., Brunt, K., Howard, S., Padman, L., and Siegfried. (2017) pyTMD: Python-based tidal prediction software (2017).
- T. S (1912) *On the Elasticity of the Earth and the Earth's Crust*. *Memoirs of the College of Science and Engineering, Kyoto Imperial University* 4:1–286
- Voigt C, Förste C, Wziontek H, et al (2016) Report on the Data Base of the International Geodynamics and Earth Tide Service (IGETS). <https://doi.org/10.2312/GFZ.B103-16087>
- Woodworth PL, Wöppelmann G, Marcos M, et al (2017) Why we must tie satellite positioning to tide gauge data. *Eos (United States)* 98
- Wöppelmann G, Marcos M (2016) Vertical land motion as a key to understanding sea level change and variability. *Reviews of Geophysics* 54
- Xu C, Xu R, Zeng W, Yan J (2020) A new high-precision gravity solid tidal model for Precision Gravity Measurement Facility. *Geod Geodyn* 11:. <https://doi.org/10.1016/j.geog.2020.04.003>
- Xu G (2007) *GPS: Theory, algorithms and applications*. *GPS: Theory, Algorithms and Applications*. <https://doi.org/10.1007/978-3-540-72715-6>
- Xu G (2010a) *Sciences of geodesy - I: Advances and future directions*
- Xu HZ (2010b) *Solid Earth Tide (in Chinese)*. Hubei Science & Technology Press
- Xu J, Sun H, Ducarme B (2004) A global experimental model for gravity tides of the Earth. *J Geodyn* 38:. <https://doi.org/10.1016/j.jog.2004.07.003>
- Xu X, Sandwell DT (2020) Toward Absolute Phase Change Recovery with InSAR: Correcting for Earth Tides and Phase Unwrapping Ambiguities. *IEEE Transactions on Geoscience and Remote Sensing* 58:. <https://doi.org/10.1109/TGRS.2019.2940207>

Yuan L, Chao BF, Ding X, Zhong P (2013) The tidal displacement field at Earth's surface determined using global GPS observations. *J Geophys Res Solid Earth* 118:2618–2632. <https://doi.org/10.1002/JGRB.50159>

Zhang CY, et al (2021) Chinese Academy of Surveying and Mapping. Scientific computation platform for geophysical geodesy